Preprints.org

Article

The Phase Diagram of the API Benzocaine and Its Highly Persistent, Metastable Crystalline Polymorphs

Ivo B. Rietveld [*] , Hiroshi Akiba , Osamu Yamamuro , María Del Barrio , René Céolin , Josep Lluís Tamarit

Article

The Phase Diagram of the API Benzocaine and Its Highly Persistent, Metastable Crystalline Polymorphs

Ivo B. Rietveld [1,2,3],*, Hiroshi Akiba [1], Osamu Yamamuro [1], Maria Barrio [4], René Céolin [4] and Josep-Lluis Tamarit [4]

[1] Institute for Solid State Physics, University of Tokyo, 5-1-5 Kashiwanoha, Kashiwa, Chiba 217-8581, Japan

[2] Université Rouen Normandie, SMS, UR 3233, F-76000 Rouen, France

[3] Faculté de pharmacie, Université Paris Cité, F-75006 Paris, France

[4] Grup de Caracterizació de Materials, Departament de Fisica, EEBE and Barcelona Research Center in Multiscale Science and Engineering, Universitat Politècnica de Catalunya, Eduard Maristany, 10-14, 08019 Barcelona, Catalonia, Spain

* Correspondence: ivo.rietveld@univ-rouen.fr

Abstract: The availability of sufficient amounts of form I of benzocaine has led to the investigation of its phase relationships with the other two existing forms II and III using adiabatic calorimetry, powder X-ray diffraction, and high-pressure differential thermal analysis. The latter two forms were known to have an enantiotropic phase relationship with form III stable at low-temperature and high-pressure, while form II is stable at room temperature. Using adiabatic calorimetry data, it can be concluded, that form I is the stable low-temperature, high-pressure form, which also happens to be stable at room temperature; however, form II, due to its persistence at room temperature, is still the most convenient polymorph to use in formulations. Form III presents a case of overall monotropy and does not possess any stability domain in the pressure-temperature phase diagram. Heat capacity data for benzocaine have been obtained by adiabatic calorimetry from 11 K up to 369 K above its melting point, which can be used to compare to results from *in-silico* crystal structure prediction.

Keywords: active pharmaceutical ingredient; phase behaviour; pressure-temperature phase diagram; thermodynamics; crystal structure; thermal expansion; adiabatic calorimetry

1. Introduction

A pressure-temperature phase diagram involving the solid phases II and III of benzocaine has been reported previously.[1] The existence of a third polymorph, form I, was known at the time, but it had not been obtained during the recrystallisation experiments and thus the phase diagram containing exclusively the forms II and III had been constructed.[1] The II-III dimorphism represents a case of enantiotropy turning into monotropy at higher pressures, where form III is the more stable form. Enantiotropy turning into monotropy was originally observed for sulphur and it is therefore also called sulphur-type phase behaviour.[2] The availability of form I makes it possible to demonstrate how its phase relationships can be incorporated in the existing pressure-temperature phase diagram and that its incorporation does not affect the phase relationships between the phases II and III.

To verify and improve the accuracy of *in-silico* crystal structure prediction, heat capacities of different polymorphs from 0 K to room temperature are of interest, so that their calculated stability hierarchies and energy contents can be compared with experimental values.[3-6] Therefore, in this paper, heat capacity data are reported starting at 10 K (with extrapolation to 0 K) for forms I and III. Both forms convert into form II around room temperature followed by melting.

The absence of form I in the formerly reported phase diagram[1] highlights the fact that polymorph II, once formed, does not convert back into form I and neither, it seems, does form III; however, as the previous paper on benzocaine demonstrates,[1] forms II and III readily interconvert.

This makes benzocaine a system of interest to study the persistence of metastable forms to help increase the solubility of a drug by using metastable forms.[7-10]

Four different crystal structures of benzocaine have been solved and can be found in the Cambridge Structural Database, although the fourth polymorph, form IV, is, at room temperature, only stable under pressure.[11] In Table 1, the crystal structures obtained under ordinary pressure (i.e., the vapour pressure of benzocaine as a function of the temperature and no applied hydrostatic pressure) have been listed. Form I crystallises in the space group $P2_1/c$ with Z = 4, form II in $P2_12_12_1$ with Z = 4, and form III in space group $P112_1$. Form IV ($P2_1/c$) appears if form I at room temperature is subjected to a pressure of about 0.50 GPa, while form I reappears at 0.41 GPa on decreasing the pressure.

**Table 1.** The crystal structures in the Cambridge Structural Database obtained at normal pressure.

Code (QQQAXG)	Form	T /K	V_{cell} /Å³	v_{spec} /cm³ g⁻¹	reference
02	I	150	871.9	0.7946	[12]
04	I	300	906.0	0.8257	[13]
06	I	300	906.0	0.8257	[14]
09	I	296	905.0	0.8248	[15]
00	II	293	910.6	0.8299	[16]
01	II	293	909.2	0.8287	[17]
05	II	300	915.0	0.8339	[13]
07	II	300	915.0	0.8339	[14]
10	II	293	912.4	0.8315	[15]
03	III	150	1759.9	0.8020	[13]
08	III	150	1759.9	0.8020	[14]

In the previous paper on the benzocaine phase diagram involving forms II and III,[1] the following calorimetric data have been reported: $T_{II \to l}$ = 362.4(5) K and $\Delta_{II \to l}H$ = 141(3) J g⁻¹ for the melting of form II and $T_{III \to II}$ = 265.3(5) K and $\Delta_{III \to II}H$ = 3.0(1.0) J g⁻¹ for the transition from form III to form II.[1] Moreover, the pressure-temperature data that have been obtained by high-pressure thermal analysis are those for the III-II transition and for the melting transition:[1]

$$P_{III\text{-}II}(T) \text{ /MPa} = -722(18) + 2.70(6) \ T \text{ /K} \tag{1}$$

$$P_{II\text{-}l}(T) \text{ /MPa} = -2166(50) + 5.99(13) \ T \text{ /K} \tag{2}$$

Commercial batches contain in general form II; however, form I can be obtained by recrystallisation from ethanol (Figure 1). The stability relationships between form I and the other two forms II and III have been investigated by adiabatic calorimetry, high-pressure differential thermal analysis and powder X-ray diffraction. With the help of the topological method,[1,18-20] a full pressure-temperature phase diagram of the trimorphism of benzocaine is presented.
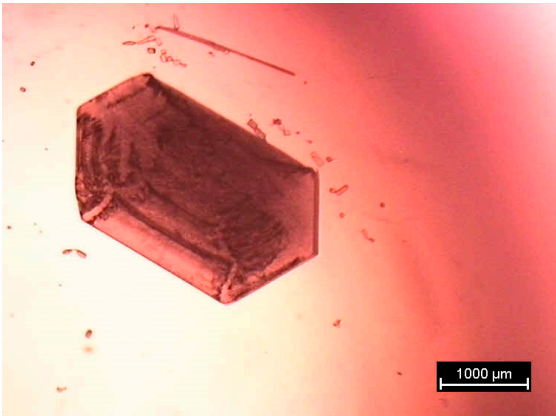
Figure 1. A photograph of a crystal of benzocaine ($C_9H_{11}NO_2$, 165.19 g mol^{-1}) form I obtained from an ethanol solution.

2. Experimental

2.1. Materials

A commercial batch of benzocaine (Sigma Aldrich, France) was recrystallised in ethanol. The obtained crystals (Figure 1) were taken out of the solution and left to dry completely under vacuum.

2.2. Adiabatic Calorimetry

The sample holder of the adiabatic calorimeter was filled with a quantity of 2.8650 g of benzocaine form I crystals, weighed on a precision balance. The description of the calorimeter has been published previously.[21] Once form I was loaded, it was cooled down to 100 K to measure the heat capacity up to room temperature. No phase transition was observed. Subsequently, heat capacity measurements from about 10 K with liquid helium were carried out up to the transition from form I into form II. After this transition, the sample was cooled down again to 100 K to measure the heat capacity and to observe the fully reversing form III to form II transition. In a final stage, the sample was cooled down to about 10 K and the heat capacity of form III and form II up to its melting and into the liquid state was obtained.

2.3. Differential Scanning Calorimetry

Differential scanning calorimetry (DSC) experiments were carried out with a conventional Q100 thermal analyser from TA Instruments. It was calibrated using the melting point of indium ($T_{fus} =$ 429.75 K and $\Delta_{fus}H = 3.267$ kJ mol^{-1}). The specimens with sample masses around 10 mg were weighed with a microbalance sensitive to 0.01 mg and sealed in aluminium pans.

In addition, a PYRIS Diamond DSC from Perkin Elmer, which uses the power compensation technique, was used for differential scanning calorimetry measurements. It was calibrated using the melting point of indium (details above) and the solid-solid phase transition of cyclohexane ($T_{II-I} =$ 186.09 K and $\Delta_{II-I}H = 6.686$ kJ mol^{-1}).

### 2.4. Powder X-ray diffraction

High-resolution X-ray diffraction as a function of temperature was performed at ordinary pressure using Debye-Scherrer geometry and transmission mode. CuKα_1 ($\lambda = 1.54056$ Å) radiation was used in a horizontally mounted INEL diffractometer with a graphite monochromator and a cylindrical position-sensitive detector (CPS-120) with 4096 channels (0.029° 2θ angular step). Powder samples were introduced into a 0.5-mm-diameter Lindemann capillary. The temperature was controlled with a 700 series Oxford Cryostream Cooler from Oxford UK Cryosystems.

Lattice parameters as a function of the temperature were determined through isothermal acquisition of X-ray patterns between 120 K and 355 K, just below the melting point of benzocaine. External calibration by means of the cubic phase $Na_2Ca_3Al_2F_4$ and cubic spline fitting was used to convert the measurement channels into 2θ. Peak positions were determined using pseudo-Voigt fitting and the unit-cell parameters were obtained from these fits.

2.5. High-pressure differential thermal analysis

High-pressure differential thermal analysis (HP-DTA) measurements were carried out with an in-house-constructed apparatus similar to the equipment built by Würflinger[22] operating between 0 and 300 MPa. Solid-solid transition temperatures between the different polymorphs of benzocaine and the melting temperatures as a function of pressure were determined for specimens mixed with an inert perfluorinated liquid (Galden; Bioblock Scientifics, Illkirch, France) to eliminate air while enclosed in tin capsules. The onset of the calorimetric peaks was taken as the transition temperature.

3. Results

3.1. The I→II transformation

Recrystallisation of benzocaine from ethanol leads to form I (P2₁/c) as testified by the resulting diffraction pattern in Figure 2. On heating, form I gradually converts into form II, which is the only form present at 353 K according to the data in Figure 2.
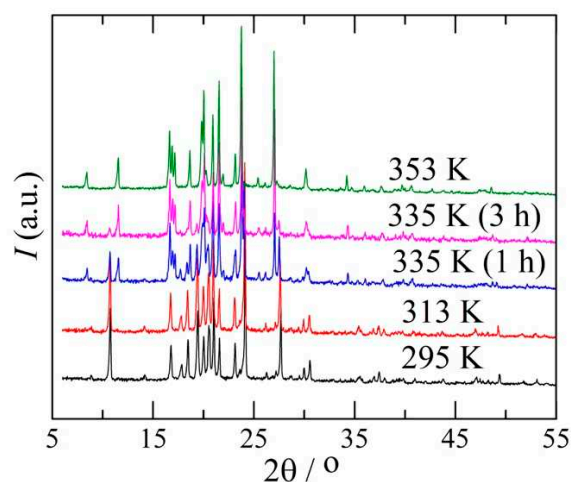
Figure 2. Benzocaine form I at 295 K (22 °C) after recrystallisation in ethanol. At 313 K (40 °C) form I still appears to be stable; however, further heating slowly leads to the formation of form II starting at 335 K (62 °C) as demonstrated by two measurements of 1 hour each at this temperature. Form II is clearly the only polymorph present at 353 K (80 °C).

It can be seen from the DSC data in Table 2 that the transformation of form I into form II is a slow and not very well controlled process. In many cases two peaks are observed and the enthalpy varies considerably. Nonetheless, the peaks can most likely be ascribed to the I → II transition based on the observations of the X-ray diffraction in Figure 2. If the peaks around 317 and 340 K are both related to the I → II transition, a clear temperature for the phase equilibrium cannot be given. The average combined enthalpy amounts to 1.6 J g⁻¹ for the TA instruments and 2.0 J g⁻¹ for the Perkin Elmer. Averaging over both machines leads to a value of 1.8 J g⁻¹, although the variability most likely indicates that the enthalpy of transition is mostly underestimated and the real transition enthalpy may be close or even above the highest observed value of 3.0 J g⁻¹ (the combined transition of sample 8 in Table 2). The melting enthalpy difference and temperature averaged over all measurements are 132(3) J g⁻¹ and 362.1(1.0) K (88.9 °C), respectively.

Table 2. Transformation of form I into form II and fusion of benzocaine form II as obtained by two differential scanning calorimeters.

		Peaks I→II				Fusion	
Sample	Mass /mg	T /K	ΔH /Jg⁻¹	T /K	ΔH /Jg⁻¹	T /K	ΔH /Jg⁻¹
			TA instruments				
1	3.84	316.8	0.67	340.2	1.09	362.6	132.9
2	3.11			341.6	0.89	362.6	137.5
3	7.89	317.0	1.70			362.8	127.4
4	1.66			340.0	1.86	362.6	129.9
5	2.42			342.4	2.63	362.6	134.4
6	3.70	318.0	0.03	344.2	1.54	362.6	133.5
7	4.44	317.6	0.50	339.2	0.61	362.6	131.0
			Perkin Elmer				

8	2.46	321.0	0.76	339.6	2.24	359.8	129.9
9	2.08	316.2	0.62	332.6	1.97	361.4	127.5
10	2.15			336.2	0.90	361.8	131.5
11	2.42			343.8	1.67	361.4	133.1

3.2. The thermal expansion of benzocaine

The unit-cell parameters of form I as a function of temperature have been compiled in Table S1 in the supplementary materials. It leads to the following expression for the specific volume of form I as a function of temperature obtained between 120 K and 320 K:

$$v_I(T) \text{ /cm}^3\text{g}^{-1} = 0.788(3) + 3.8(2.2) \times 10^{-5}\ T/\text{K} + 3.0(5) \times 10^{-7}\ T^2/\text{K} \tag{3}$$

Within the fitting range the average deviation of this expression in relation to the measured data is less than 0.1%.

To ensure that the volume differences between the polymorphs are consistent, the diffraction of the other two polymorphs has been measured with the same experimental settings and with the same sample as form I. These specific volumes match within error the previously obtained data.[1] The unit-cell parameters of forms II and III as a function of temperature can be found in Tables S2 and S3 respectively in the supplementary materials. These data lead to the following expressions for the specific volume of forms II and III of benzocaine:

$$v_{II}(T) \text{ /cm}^3\text{g}^{-1} = 0.835(30) - 2.19(1.99) \times 10^{-4}\ T/\text{K} + 7.15(3.27) \times 10^{-7}\ T/\text{K} \tag{4}$$

$$v_{III}(T) \text{ /cm}^3\text{g}^{-1} = 0.798(3) - 2.78(2.85) \times 10^{-5}\ T/\text{K} + 4.91(74) \times 10^{-7}\ T/\text{K} \tag{5}$$

The average error of these fits within their fitting ranges is 0.13% (form II, 250 K – 355 K) and 0.05% (form III, 120 K – 255 K). Moreover, it can be seen in Figure 3 that form I is the densest form (eq. 3) as it has the lowest specific volume from the lowest measured temperature up to its equilibrium with form II. Form III has a slightly lower density (eq. 5) and the least dense form is form II (eq. 4).
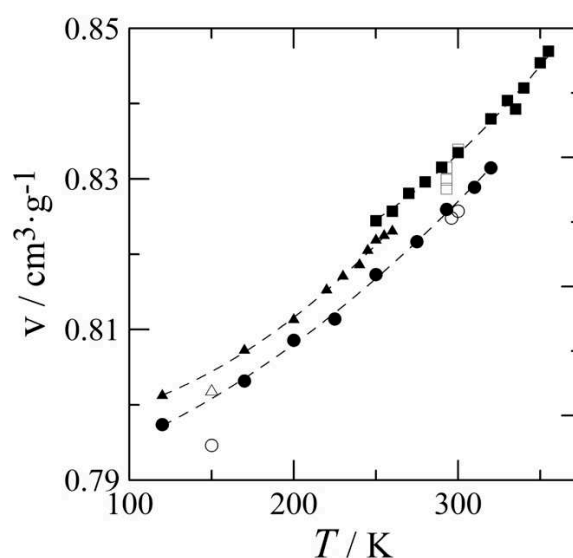
Figure 3. Specific volume of forms I (filled circles), II (filled squares), and III (filled triangles) obtained by powder X-ray diffraction in the current study. Literature data of single crystal data indicated by open symbols.

3.3. Heat capacity, entropy, enthalpy, and Gibbs free energy obtained by adiabatic calorimetry
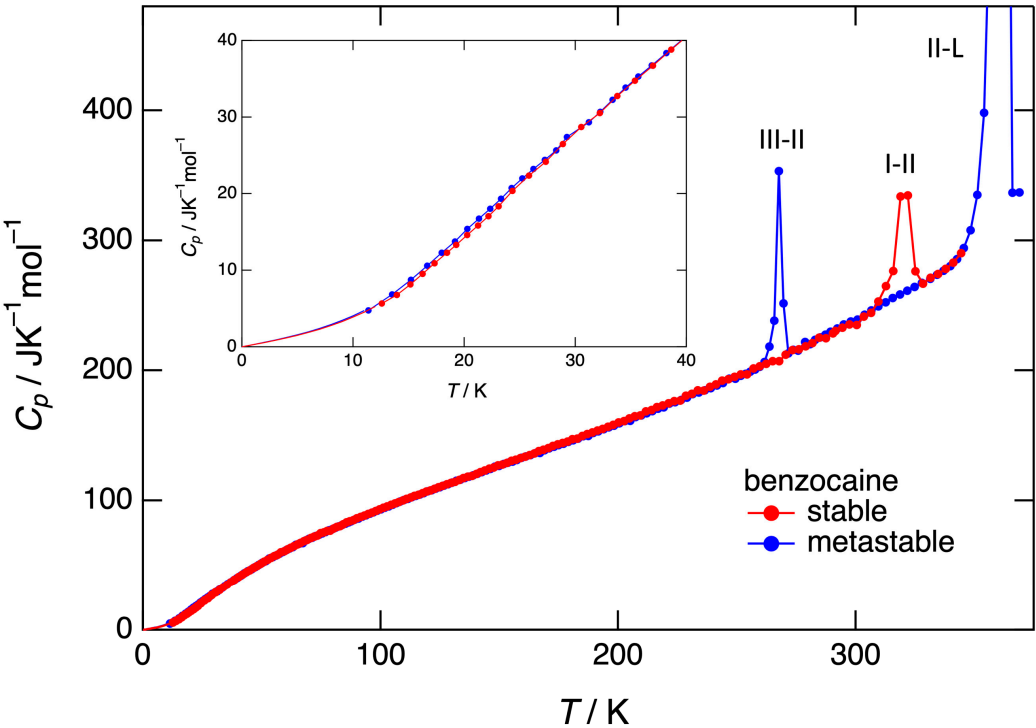
The heat capacity of form I has been measured by adiabatic calorimetry from 12.6 K on, while the heat capacity below that temperature has been obtained by extrapolation with equation S1 (see Figure 4 and Table S4 in the Supplementary Materials). Form I turns into form II at 319.5 K as

indicated by the relatively broad peak (red line in Figure 4), which compares with the slow conversion of form I into form II as observed by DSC. The entropy and enthalpy involved with this transformation and obtained by adiabatic calorimetry can be found in Table 3.

Table 3. Temperature, entropy, and enthalpy of transition obtained with adiabatic calorimetry.

| Equilibrium	T /K	ΔS /J g^{-1} K^{-1}	ΔH /J g^{-1}
III-II	266.0	0.010225	2.7194
I-II	319.5	0.011938	3.8146
II-*l*	361.0	0.369514	133.412

Figure 4. Heat capacity data of forms I (red) and III (blue), turning into form II at the respective peaks followed by the melting peak.

Once converted into form II, the heat capacity was once again measured from 11.4 K on, with an extrapolation to 0 K by eq. S2 in the supplementary materials. The data can be found in Table S4 in the supplementary materials. Form II on cooling turns into form III, which is the actual polymorph measured at low temperature. A peak is observed (blue line in Figure 4) at 266.0 K indicating the transition from form III to form II, which then melts at 361.0 K. The entropy and enthalpy changes of the two transitions obtained by adiabatic calorimetry have been compiled in Table 3.

3.4. Transition temperatures obtained under pressure

The analysis of the pressure-temperature phase diagram, which will follow in the discussion led to the realisation that the I-II and I-*l* phase equilibria were accessible for measurement in the high-pressure differential thermal analyser. Hence, samples of form I have been loaded in tin capsules and measurements as a function of temperature for a given pressure have been carried out. Moreover, further analysis of the phase diagram demonstrated that form I could be regained through crystallising the melt at high pressure and cooling down. Peaks indicating that form I is obtained again can be observed in Figure 5.
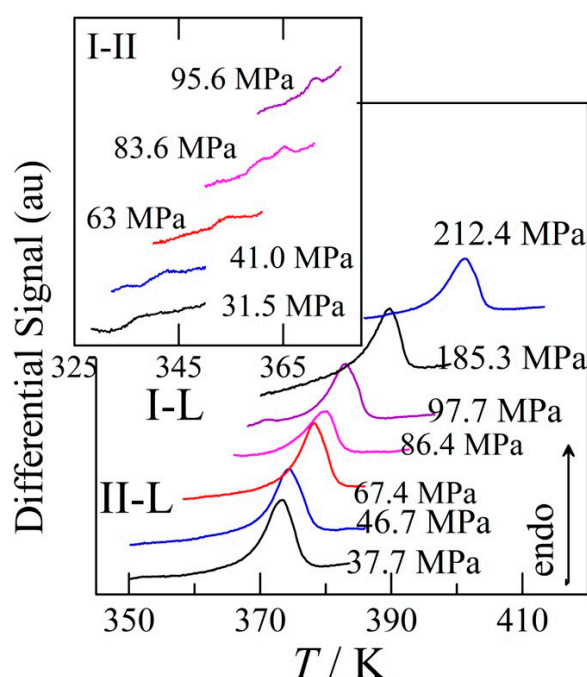
Figure 5. High-pressure differential thermal analysis of the I-II transition (inset) and melting peaks of either form II (lower pressure) or form I (higher pressure).

The transition pressures as a function of temperature of the two-phase equilibria I-II, II-*l*, and I-*l* obtained by HP-DTA in the current study have been compiled in Table S5 in the supplementary materials. They result in the following equations of the transition pressure (P /MPa) fitted to the data:

$$P_{I-II} \text{ /MPa} = -598(22) + 1.89(7) \text{ T /K} \qquad R^2 = 0.992 \qquad (6)$$

$$P_{II-l} \text{ /MPa} = -2350(128) + 6.5(4) \text{ T /K} \qquad R^2 = 0.98 \qquad (7)$$

$$P_{I-l} \text{ /MPa} = -2131(121) + 5.9(3) \text{ T /K} \qquad R^2 = 0.989 \qquad (8)$$

4. Discussion

4.1. Stability of benzocaine under ordinary pressure, adiabatic versus DSC

The stability of the different polymorphs can be directly obtained from the heat capacity data, which have been converted to entropy, enthalpy, and Gibbs free energy in the Tables S6 and S7 in the supplementary materials. The Gibbs free energy of form I has been set to zero at 0 K, resulting in a positive Gibbs free energy of 197.4 J mol^{-1} for form III. The Gibbs free energies of forms III and II meet at 266 K and there should be a slight change in the slope in the blue curve in Figure 6. The Gibbs free energy of form I meets that of form II at 319.5 K, where both the red curve and the blue curve in Figure 6 become identical. A final change in the slope of the blue curve should occur at 361.0 K, where form II is replaced by the liquid as the most stable phase.

Comparison between Tables 2 and 3 demonstrates that the I-II transition possesses indeed a higher transition enthalpy than obtained by DSC, which is probably due to the fact that part of the solid-solid transition is not fully observed by DSC, because the signal may be spread over a larger temperature domain and fade into the baseline. This highlights the importance of the adiabatic calorimetry, which provides clearly better equilibrium data for slow solid-solid transitions. The melting enthalpy obtained with the recent batches is slightly smaller for the values obtained by DSC, although the scatter is relatively large and within measurement error, the DSC and adiabatic calorimetric melting data are the same. The previously published DSC data on forms II and III appear

to be a little higher than the adiabatic calorimetric data. The reason for this is not clear. The calibration of the DSC will have been different and a different batch for the measurements was used.
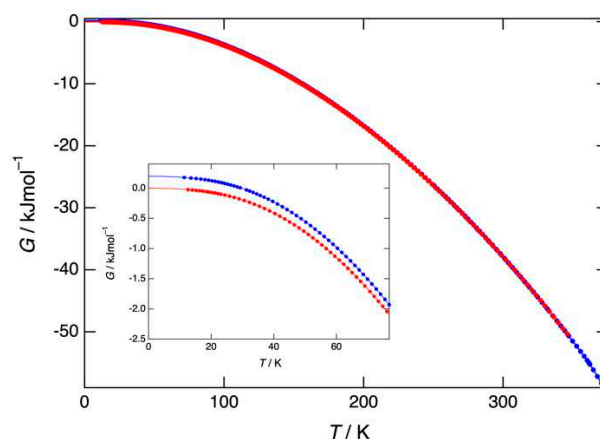

Figure 6. Gibbs free energy of form I (red) and form III (blue), which become equal once both forms have turned into form II. Form III has a higher Gibbs free energy and is therefore less stable than form I. Form I remains the most stable form up to 319.5 K.

4.2. Construction of the pressure-temperature phase diagram

4.2.1. High-pressure data and its triple points

In Figure 7, the high-pressure data (solid circles) and the fitted lines (eqs. 1, 6-8) have been plotted. The previously measured II-*l* equilibrium (eq. 2) has not been used, because the fit may have been based on the melting equilibria of both form I and form II. It can be seen that both II-*l* and I-*l* (eqs. 7 and 8 respectively) are very close to the former equilibrium eq. 2. From this experimental phase diagram, it is immediately clear that at 0 MPa, form II melts at the highest temperature (purple line) and that a stable I-II equilibrium occurs slightly above 300 K. The blue-purple triangle that is formed with the dashed 0 MPa baseline represents the small P-T domain in which form II is stable. Form I is stable on the upper left-hand side of the blue line and the III-II equilibrium, the green line, must be metastable. Because form I is stable above the blue I-II equilibrium, the red dotted line, representing the melting of form I, becomes stable once it intersects the blue line towards higher pressures, while it is found at the right-hand side of the purple II-*l* equilibrium. The intersection of the blue, purple and red lines is the stable I-II-*l* triple point of which the coordinates are listed in Table 4 below. Moreover, the intersection of the green III-II and purple II-*l* equilibria provides the position of the III-II-*l* triple point. Finally, the green III-II and blue I-II equilibria intersect at negative pressure at the I-II-III triple point. Each intersection of the four two-phase equilibria with their respective vapour phase pressure, close to 0 MPa (and approximated by the dashed black line), represents a triple point involving the vapour phase *v* (Table 4, in order of increasing temperature): III-II-*v*, I-II-*v*, I-*l*-*v*, II-*l*-*v*. Here, the triple point temperature of III-II-*v* is determined with eq. 1, which value at 0 MPa equals 267.8 K. For the triple point I-II-*v*, eq. 6 is used, leading to a temperature of 316.6 K. In the same way the triple point of II-*l*-*v* is determined with eq. 8, leading to 359.5 K, while the triple point temperature II-*l*-*v* follows from eq. 7 and gives rise to 362.0 K. The calculations of the triple points have been carried out with the equations of which the parameters have not been rounded off and the resulting triple point temperatures may therefore differ slightly if the equations are used as listed in this paper.
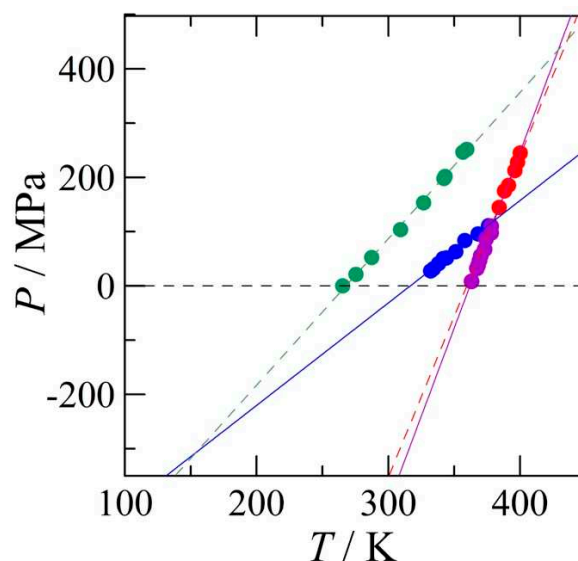
Figure 7. The pressure-temperature phase diagram based exclusively on the obtained HP-DTA data measured in the current study (equilibrium I-II dark blue, equilibrium II-*l* purple, equilibrium I-*l* red) and previously measured data (equilibrium III-II green).[1].

The remaining question is the position of the I-III equilibrium and connected to this, the position of the III-*l* equilibrium. This will be solved in a topological manner as discussed in the next section.

4.2.2. The positions of the I-III and the III-L equilibria

The positions of the I-III and the III-*l* equilibria in the phase diagram are closely linked. It is, however, easiest to locate the I-III equilibrium, because its position has the more dramatic consequences for the phase behaviour of benzocaine. In Figure 7, there is one triple point, I-II-III, at low temperature and negative pressure, which must be intersected by the I-III equilibrium. From eqs. 3 and 5 and Figure 8, it can be seen that form I has the smaller volume, thus form I is according to Le Chatelier the stable high-pressure form in relation to form III. The differences in entropy of the polymorphs I and III in relation to form II are listed in Table 3. The entropy change going from form III to II is smaller than the entropy change of form I to II. This implies that form III contains more entropy and is therefore the high-temperature form in relation to form I. The same conclusion can be reached by comparing the entropies listed in the tables S6 (form I) and S7 (form III). Thus, simply considering the global inequalities in the volume and the entropy, it is found that in relation to the I-III equilibrium, form I is the low-temperature, high-pressure form and form III is the high-temperature, low-pressure form; in other words, any phase equilibrium between the two polymorphs has a positive slope with on the upper left-hand side form I and on the lower right-hand side form III.

Taking the I-II-III triple point (T = 154 K and P = -307 MPa) as a pivot for the I-III equilibrium and taking into consideration its positive slope, three topological scenarios exist: (1) I-III with a steeper slope than III-II and I-II, (2) I-III with a less steep slope than III-II, but a steeper slope than I-II and (3) I-III with a shallower slope than both other solid-solid equilibria. It should be kept in mind that form I is stable above the equilibrium and form III below. In the case of scenario (1), form I will be stable at high pressure and low temperature, form III will appear on crossing this equilibrium, which will then turn into form II on crossing from top left the III-II equilibrium; however, at that point form II is still metastable with respect to form I and that implies that form III is also still metastable with respect to form I, which creates an inconsistency in the phase behaviour. A similar inconsistency exists for scenario (2): form I, which is stable according to the phase diagram in Figure 7, turns into form III, which must be metastable, because form II is the more stable form. This implies that form I must be metastable towards form II, but that only occurs once the blue I-II equilibrium is crossed. Thus, the only viable scenario is number (3) for which the slope of the III-I equilibrium is the

smallest of the three solid-solid equilibria and the line is therefore found below the I-II phase equilibrium. This also implies that the I-III equilibrium is completely metastable, because neither form I nor form III are stable below the I-II equilibrium and it implies that Figure 7 already covers the full stable phase diagram. The remaining unknown is the slope of the I-III equilibrium and where precisely it intersects the vapour phase pressure close to 0 MPa, which would represent the I-III transition under ordinary conditions (i.e., in the calorimeter).

There are several approaches to estimate the slope of the I-III equilibrium of which the following two are the most direct: (1) by calculating the slope using the Clapeyron equation, or (2) by calculating the I-III-v (v = vapour) triple point, the transition temperature at ordinary pressure (0 MPa) using an equation proposed by Yu.[23] With option (1), the slope with the I-II-III triple point will define the position of the equilibrium expressed as a straight line and with option (2) a straight line drawn through the two triple points I-II-III and I-III-v will define the position of the equilibrium. Because both are abstract extrapolations, neither will necessarily represent the realistically precise position of the equilibrium, but topologically, it will provide the correct interpretation of the phase behaviour, which should be thermodynamically consistent.

Using option (1), the calculation of the slope, necessitates the Clapeyron equation:

$$\frac{dP}{dT} = \frac{\Delta S}{\Delta v} \tag{9}$$

in which dP/dT is the slope in the pressure-temperature phase diagram, ΔS is the entropy difference and Δv is the volume difference between the two phases I and III. ΔS follows from Table 3 (or the Tables S6 and S7 in the supplementary materials) and is $\Delta_{I \to III}S = \Delta_{I \to II}S - \Delta_{III \to II}S = 0.011938 - 0.010225 = 0.001713$ J g^{-1} K^{-1}. For the difference in volume, in the ideal case the volume at the transition temperature under ordinary conditions should be taken, but this value is unknown and located at a higher temperature than where forms III and I can be obtained. Therefore, it is more convenient to choose a temperature at which both volumes are accurately defined, such as 225 K using the eqs. 3 and 5. This leads to $v_I = 0.81221$ cm^3 g^{-1} and $v_{III} = 0.81613$ cm^3 g^{-1} and thus to a difference of $\Delta_{I \to III}v = v_{III} - v_I = 0.00392$ cm^{3}g^{-1}. Using the Clapeyron equation eq. 9, this leads to a slope of 0.4375 MPa K^{-1} and using the triple point I-II-III (Table 4) a tentative equation for the I-III equilibrium is obtained: P_{I-III} /MPa = -374 + 0.437 T /K. It can be seen that the slope is indeed much less than that of the III-II equilibrium (eq. 1) with 2.70 MPa K^{-1} or the I-II equilibrium with 1.89 MPa K^{-1} (eq. 6). Through this equation for the I-III equilibrium, the triple point temperature of I-III-v is found to be 856 K.

Using option (2) requires an equation proposed by Yu to calculate the solid-solid transition temperature:[23]

$$T_{I \to III} = \frac{\Delta_{III \to l}H - \Delta_{I \to l}H}{\Delta_{III \to l}S - \Delta_{I \to l}S} = \frac{\Delta_{II \to l}H + \Delta_{III \to II}H - (\Delta_{II \to l}H + \Delta_{I \to II}H)}{\Delta_{II \to l}S + \Delta_{III \to II}S - (\Delta_{II \to l}S + \Delta_{I \to II}S)} = \frac{\Delta_{III \to II}H - \Delta_{I \to II}H}{\Delta_{III \to II}S - \Delta_{I \to II}S} \tag{10}$$

As most of the transition enthalpies and entropies are not known, because only the fusion of form II has been measured, eq. 10 has been rewritten to provide the transition temperature between forms I and III using form II instead of the liquid phase, which is thermodynamically completely equivalent to the proposed equation by Yu involving the liquid phase. This leads to a temperature for the I-III-v triple point of 639 K. As this is at "ordinary pressure", the pressure value will be approximated with 0 MPa. Then, with the I-II-III triple point at 154 K and -307 MPa, the following equation for the I-III equilibrium can be obtained: P_{I-III} /MPa = -404 + 0.633 T /K. Again, it can be seen that the slope is rather small and much less than the slopes of the I-II and II-III equilibria and the two scenarios can be considered to roughly represent the error margin of the I-III equilibrium, which will always be metastable and out of reach of measurement.

To draw the topological phase diagram, the latter expression will be chosen (there is no scientific ground to choose one expression over the other):

$$P_{I-III} \text{ /MPa} = -404 + 0.633 \; T \text{ /K} \tag{11}$$

Once the position of the I-III equilibrium has been defined, it also defines the position of the melting equilibrium of form III, because the I-III equilibrium will intersect the I-l equilibrium leading to the triple point I-III-l. Thus, with eqs. 8 and 11, the following coordinates are found: 326 K and -198 MPa.

Another triple point of the III-*l* equilibrium is III-II-*l*, which can be calculated with the equations obtained by measurement eqs. 1 and 7. The triple point coordinates are 429 K and 435 MPa. The III-*l* equilibrium passing through these two points, possesses therefore the following equation:

$$P_{III\text{-}l} / \text{MPa} = -2204 + 6.15\, T\, /\text{K} \tag{12}$$

Using this equation, the melting point of form III can be determined as this will occur at 0 MPa (ordinary pressure), leading to 358.3 K. This value, obtained by extrapolation of the topological phase diagram can be compared with the melting point that would be obtained by the equation proposed by Yu, but then modified to obtain a melting transition:[1]

$$T_{III\to l} = \frac{\Delta_{II\to l}H + \Delta_{III\to II}H}{\frac{\Delta_{II\to l}H}{T_{II\to l}} + \frac{\Delta_{III\to II}H}{T_{III\to II}}} = \frac{\Delta_{II\to l}H + \Delta_{III\to II}H}{\Delta_{II\to l}S + \Delta_{III\to II}S} \tag{13}$$

Using the values from Table 3, this leads to the melting point of form III of 358.5 K, so the differences in this case are negligible. It can also be concluded that form III is the lowest melting form, followed by form I, while form II is the highest melting form (Table 4). Another observation that can be made is that the slope of the II-*l* equilibrium, 6.5 MPa K^{-1}, is the steepest slope, while III-*l* has a slightly shallower slope of 6.15 MPa K^{-1} and form I has the gentlest slope with 5.9 MPa K^{-1}. This sequence in slopes leads to a stable melting equilibrium for form I at high pressure, whereas the melting equilibrium of form III is placed in such a way that it never becomes stable reflecting the metastability of form III.

4.2.3. The pressure-temperature phase diagram

In a pressure-temperature phase diagram with three solid phases, the liquid, and the vapour phase, ten triple points must be present, that represent the ten possible intersections between the six two-phase equilibria.[24] All triple points have been listed in Table 4, based on the measured phase equilibrium data with the high-pressure differential thermal analysis. Only, when necessary, as in the case of the slope of the I-III equilibrium enthalpy and entropy values obtained by adiabatic calorimetry have been used. Therefore, there are small differences between the transition temperatures obtained by HP-DTA and DSC or adiabatic calorimetry, which can be considered the uncertainty over the measurements. Moreover, it is possible to calculate the vapour pressure of the condensed phases using the Clausius-Clapeyron equation and the boiling temperature and enthalpy of vaporization obtained through ACD-Labs,[25] as it has previously been carried out for the equilibria involving the vapour phase and forms II and III.[1] This approach is explained in detail in the supplementary materials. The calculated vapour pressures of the respective triple points have been compiled in Table 4 (see also Tables S8 and S9 in the supplementary materials).

The resulting topological phase diagram is presented in Figure 8. For the sake of clarity, the melting equilibria (triple points 1, 2, and 3) have been separated in an exaggerated way. The stable vapour phase equilibria defining the lower limit of the stable condensed phases are given by the sequence f-7-1-a. The stability domain of form II is defined by the black triangle 1-4-7 and above this triangle f-7-4-c defines the stability domain of form I. Form III becomes more stable than form I below the equilibrium line indicated by 'j', but its position is such that the vapour phase has the lowest Gibbs free energy and is thus the more stable phase.

Table 4. Triple points involving polymorphs I, II, and III of benzocaine.

Triple point	Temperature /K	Pressure /Pa	
I-II-III	154.0	-307×10^6	metastable
III-II-*v*	267.8	0.012	metastable
I-II-*v*	316.6	2.4	stable
I-III-*l*	326.1	-198×10^6	supermetastable
III-*l*-*v*	358.3	78	supermetastable
I-*l*-*v*	359.5	83	metastable

II-*l-v*	362.0	95	stable
I-II-*l*	380.1	120×10^6	stable
III-II-*l*	428.9	435×10^6	metastable
I-III-*v*	639.3	7.4×10^6	supermetastable
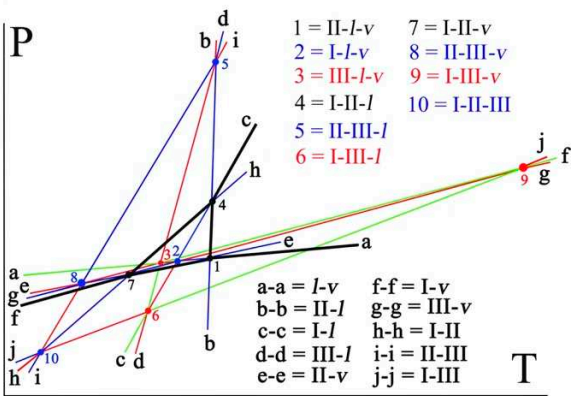
Figure 8. Topological phase diagram of the three polymorphs of benzocaine together with the liquid and the vapour phase. The 10 triple points have been numbered and listed in the graph as are the different two-phase equilibrium lines. Black indicates stable, blue metastable, red supermetastable and green hypermetastable. Form I is stable in the upper left-hand corner defined by the black lines, the liquid is stable in the upper right-hand corner defined by the black lines, the vapour is stable below the black lines and form II is stable within the triangle formed by the black lines. A close-up of the triple points 1, 2, 3, 7, and 8 involving the vapour phase equilibria can be found in Figure S1 in the supplementary materials.

Although the phase diagram involving three phases seems rather complicated, it should be realised that it consists of a sum of three dimorphism phase diagrams. The first being the previously published III-II phase diagram, where both form III and form II have a stable temperature domain at ordinary pressure (enantiotropy), whereas the system becomes monotropic at higher pressures (see blue lines and point 5 in Figure 8) with form III the single more stable form. This phase behaviour is similar to that of sulphur.[2] The second phase diagram is that of forms I and II, which presents a very similar behaviour as forms II and III, except that now form I is the high pressure form (see black lines in Figure 8). As both form I and form III compete for the high-pressure, low-temperature domain, the third phase diagram, that of forms I and III, demonstrates that form III is less stable than form I. In fact, when form III finally has a lower Gibbs energy than form I, it is always the vapour that possesses an even lower Gibbs energy. The I-III equilibrium is indicated by the line j-j, which is mostly green (hypermetastable). Due to the overall monotropy between forms I and III, form III does not possess any stable pressure-temperature domain.

Pressure-temperature phase diagrams related to dimorphism are relatively easy to understand, because they only contain four triple points and therefore only four possible cases exists, which have been described by Bakhuis Roozeboom.[2] These four cases are overall monotropy (benzocaine I-III), overall enantiotropy, as in the case of gestodene,[26] enantiotropy turning monotropic on increasing pressure (benzocaine II-III and I-II) and the inverse case, monotropy turning enantiotropic on increasing pressure of which ritonavir is an example.[19] The four resulting pressure-temperature phase diagrams can be found in a recently published paper.[27]

Trimorphism, Figure 8, becomes rapidly more complicated to describe than dimorphism and in the literature only four other papers report on topological phase diagrams involving trimorphism[28-31] and one other concerning tetramorphism.[10] In the case of the trimorphism of ferrocene,[28] one of the phases is also overall metastable, but whereas for benzocaine, the system is enantiotropic at low pressure and becomes monotropic at higher pressure, like sulphur,[2] for ferrocene the two other phases are overall enantiotropic exhibiting stable domains irrespective of the pressure. For piracetam, all three forms have their stable domain, but only one remains stable under higher pressure, i.e., the

system becomes fully monotropic.[29] In the case of 2-methyl-2-chloropropane, two solid phases are overall enantiotropic, whereas the third one becomes monotropic at high pressure.[31] In the case of l-tyrosine ethyl ester, again a sulphur type phase behaviour between two phases is encountered, whereas the third phase appears to exhibit a stable domain at extremely low temperature, so all three phases are stable in their respective temperature domain at low pressure.[30] A similar line-up of stability domains as a function of temperature is observed for tetramorphic pyrazinamide, while under higher pressure, only two polymorphs remain.[10] Thus, even within this small collection of samples, many different combinations of phase behaviour are encountered.

5. Conclusions

Adiabatic calorimetry and high-pressure differential thermal analysis both lead to the conclusion that benzocaine form I possesses the largest stability domain and that form II is only stable in a small pressure-temperature domain before melting. Full consistency exists between the outcomes of the two methods. A combination of the adiabatic calorimetry with powder X-ray diffraction for the specific volumes and the high-pressure measurements has led to a complete topological pressure-temperature phase diagram (Figure 8), in which it is demonstrated that form III does not possess any stable domain (Figures 8 and S1 in the supplementary materials). This case is a prime example of how phase behaviour can be added up and that the relative hierarchy between phases doesn't change, while the absolute hierarchy is adapted as a function of the stability behaviour of a new phase. Form IV,[11] for example, can be added to this phase diagram, once more information about its phase relationship with form I is obtained.

Even though form I is not the commercially available polymorph, adiabatic calorimetry has demonstrated that it is the most stable form from 0 K up to T_{I-II} = 319.5 K. Nonetheless, form II is the commercial form, and it does not appear to transform at all into form I under ordinary conditions at room temperature despite its metastable character with respect to form I. The only way to obtain form I appears to be through crystallisation from ethanol. However, while constructing the topological phase diagram of benzocaine, it became clear that the I-II-l triple point (point 4 in Figure 8) was in reach of the limits of the HP-DTA equipment and that the melting equilibrium of form I could be observed. This has also led to the assumption that by melting form II, increasing the pressure, and lowering the temperature once above the I-II-l triple point pressure, form I may crystallise instead of form II. The appearance of the I-II transition in subsequent runs confirmed this assumption (Figure 5).

Interestingly, form III, which appeared to be a low-temperature, high-pressure polymorph, at least with respect to form II,[1] is in fact a high temperature, low pressure form in relation to the more stable form I. The reason that form III appears at all is that once polymorph II has formed, it has never been observed to convert back into form I; therefore, commercial batches contain form II. Due to this persistence, form III can appear at low temperatures, as a means for the system to lower its energy towards form I even if the system remains trapped as a direct transition between form I and form III has never been observed either.

For pharmaceutical applications, these findings imply that form II can be safely used for the development of solid-state formulations. This would render the formulations safe against high temperatures. The reason why the polymorphs II and III are so persistent in relation to a more stable form should be investigated more thoroughly, so that such behaviour may be programmed into a drug molecule through synthesis.

References

1. Gana, I.; Barrio, M.; Do, B.; Tamarit, J.-L.; Céolin, R.; Rietveld, I. B., Benzocaine polymorphism: Pressure-temperature phase diagram involving forms II and III. *Int. J. Pharm.* **2013,** 456, 480-488.

2. Bakhuis Roozeboom, H. W., *Die heterogenen Gleichgewichte vom Standpunkte der Phasenlehre. Erstes Heft: Die Phasenlehre - Systeme aus einer Komponente.* ed.; Friedrich Vieweg und Sohn: Braunschweig, 1901; Vol. 1.

3. Reilly, A. M.; Cooper, R. I.; Adjiman, C. S.; Bhattacharya, S.; Boese, A. D.; Brandenburg, J. G.; Bygrave, P. J.; Bylsma, R.; Campbell, J. E.; Car, R.; Case, D. H.; Chadha, R.; Cole, J. C.; Cosburn, K.; Cuppen, H. M.; Curtis, F.; Day, G. M.; DiStasio Jr, R. A.; Dzyabchenko, A.; van Eijck, B. P.; Elking, D. M.; van den Ende, J. A.; Facelli, J. C.; Ferraro, M. B.; Fusti-Molnar, L.; Gatsiou, C.-A.; Gee, T. S.; de Gelder, R.; Ghiringhelli, L. M.; Goto, H.; Grimme, S.; Guo, R.; Hofmann, D. W. M.; Hoja, J.; Hylton, R. K.; Iuzzolino, L.; Jankiewicz, W.; de Jong, D. T.; Kendrick, J.; de Klerk, N. J. J.; Ko, H.-Y.; Kuleshova, L. N.; Li, X.; Lohani, S.; Leusen, F. J. J.; Lund, A. M.; Lv, J.; Ma, Y.; Marom, N.; Masunov, A. E.; McCabe, P.; McMahon, D. P.; Meekes, H.; Metz, M. P.; Misquitta, A. J.; Mohamed, S.; Monserrat, B.; Needs, R. J.; Neumann, M. A.; Nyman, J.; Obata, S.; Oberhofer, H.; Oganov, A. R.; Orendt, A. M.; Pagola, G. I.; Pantelides, C. C.; Pickard, C. J.; Podeszwa, R.; Price, L. S.; Price, S. L.; Pulido, A.; Read, M. G.; Reuter, K.; Schneider, E.; Schober, C.; Shields, G. P.; Singh, P.; Sugden, I. J.; Szalewicz, K.; Taylor, C. R.; Tkatchenko, A.; Tuckerman, M. E.; Vacarro, F.; Vasileiadis, M.; Vazquez-Mayagoitia, A.; Vogt, L.; Wang, Y.; Watson, R. E.; de Wijs, G. A.; Yang, J.; Zhu, Q.; Groom, C. R., Report on the sixth blind test of organic crystal structure prediction methods. *Acta Crystallogr. B* **2016,** 72, 439-459.

4. Addicoat, M.; Adjiman, C. S.; Arhangelskis, M.; Beran, G. J. O.; Bowskill, D.; Brandenburg, J. G.; Braun, D. E.; Burger, V.; Cole, J.; Cruz-Cabeza, A. J.; Day, G. M.; Deringer, V. L.; Guo, R.; Hare, A.; Helfferich, J.; Hoja, J.; Iuzzolino, L.; Jobbins, S.; Marom, N.; McKay, D.; Mitchell, J. B. O.; Mohamed, S.; Neumann, M.; Nilsson Lill, S.; Nyman, J.; Oganov, A. R.; Piaggi, P.; Price, S. L.; Reutzel-Edens, S.; Rietveld, I.; Ruggiero, M.; Ryder, M. R.; Sastre, G.; Schon, J. C.; Taylor, C.; Tkatchenko, A.; Tsuzuki, S.; van den Ende, J.; Woodley, S. M.; Woollam, G.; Zhu, Q., Crystal structure evaluation: calculating relative stabilities and other criteria: general discussion. *Faraday Discuss.* **2018**.

5. Sun, G.; Liu, X.; Abramov, Y. A.; Nilsson Lill, S. O.; Chang, C.; Burger, V.; Broo, A., Current State-of-the-art In-house and Cloud-Based Applications of Virtual Polymorph Screening of Pharmaceutical Compounds: A Challenging Case of AZD1305. *Cryst. Growth Des.* **2021,** 21, 1972-1983.

6. Neumann, M. A.; van de Streek, J.; Fabbiani, F. P. A.; Hidber, P.; Grassmann, O., Combined crystal structure prediction and high-pressure crystallization in rational pharmaceutical polymorph screening. *Nat. Commun.* **2015,** 6, 7793-7799.

7. Baaklini, G.; Dupray, V.; Coquerel, G., Inhibition of the spontaneous polymorphic transition of pyrazinamide γ form at room temperature by co-spray drying with 1,3-dimethylurea. *Int. J. Pharm. (Amsterdam, Neth.)* **2015,** 479, 163-170.

8. Smets, M. M. H.; Baaklini, G.; Tijink, A.; Sweers, L.; Vossen, C. H. F.; Brandel, C.; Meekes, H.; Cuppen, H. M.; Coquerel, G., Inhibition of the Vapor-Mediated Phase Transition of the High Temperature Form of Pyrazinamide. *Cryst. Growth Des.* **2018,** 18, 1109-1116.

9. Li, K.; Gbabode, G.; Barrio, M.; Tamarit, J.-L.; Vergé-Depré, M.; Robert, B.; Rietveld, I. B., The phase relationship between the pyrazinamide polymorphs α and γ. *Int. J. Pharm.* **2020,** 580, 119230.

10. Li, K.; Gbabode, G.; Vergé-Depré, M.; Robert, B.; Barrio, M.; Itié, J.-P.; Tamarit, J.-L.; Rietveld, I. B., The pressure–temperature phase diagram of tetramorphic pyrazinamide. *CrystEngComm* **2022,** 24, 5041-5051.

11. Patyk-Kazmierczak, E.; Kazmierczak, M., A new high-pressure benzocaine polymorph - towards understanding the molecular aggregation in crystals of an important active pharmaceutical ingredient (API). *Acta Crystallogr. B* **2020,** 76, 56-64.

12. Lynch, D. E.; McClenaghan, I., Monoclinic form of ethyl 4-aminobenzoate (benzocaine). *Acta Crystallogr. E* **2002,** 58, O708-O709.

13. Chan, E. J.; Rae, A. D.; Welberry, T. R., On the polymorphism of benzocaine; a low-temperature structural phase transition for form (II). *Acta Crystallogr. B* **2009,** 65, 509-515.

14. Chan, E. J.; Welberry, T. R., Precursor effects of the orthorhombic to monoclinic phase transition in benzocaine form (II) revealed by X-ray diffuse scattering. *Acta Crystallogr. B* **2010,** 66, 260-270.

15. Patel, M. A.; AbouGhaly, M. H. H.; Chadwick, K., The discovery and investigation of a crystalline solid solution of an active pharmaceutical ingredient. *Int. J. Pharm.* **2017,** 532, 166-176.

16. Baptista, A., Radiocrystallographic study of organic substances. III. Benzocaine. *Anais da Academia Brasileira de Ciencias* **1968,** 40, 67-70.

17. Sinha, B. K.; Pattabhi, V., Crystal-Structure of Benzocaine-a Local-Anesthetic. *P Indian as-Chem Sci* **1987,** 98, 229-234.

18. Rietveld, I. B.; Ceolin, R., Rotigotine: Unexpected Polymorphism with Predictable Overall Monotropic Behavior. *J. Pharm. Sci.* **2015,** 104, 4117-4122.

19. Céolin, R.; Rietveld, I. B., The topological pressure-temperature phase diagram of ritonavir, an extraordinary case of crystalline dimorphism. *Ann. Pharm. Fr.* **2015,** 73, 22-30.

20. Bauer, M.; Lacoulonche, F.; Ceolin, R.; Barrio, M.; Khichane, I.; Robert, B.; Tamarit, J. L.; Rietveld, I. B., On the dimorphism of prednisolone: The topological pressure-temperature phase diagram involving forms I and II. *Int. J. Pharm.* **2022,** 624, 122047.

21. Tsukushi, I.; Yamamuro, O.; Sadanami, K.; Nishizawa, M.; Matsuo, T.; Takeda, K., Construction of a top-loading adiabatic calorimeter and enthalpy relaxation of glassy (1,3-propanediol)0.5(1,2-propanediamine)0.5. *Rev. Sci. Instrum.* **1998,** 69, 179-184.

22. Würflinger, A., Differential thermal-analysis under high-pressure IV. Low-temperature DTA of solid-solid and solid-liquid transitions of several hydrocarbons up to 3 kbar. *Ber. Bunsen-Ges. Phys. Chem.* **1975,** 79, 1195-1201.

23. Yu, L., Inferring Thermodynamic Stability Relationship of Polymorphs from Melting Data. *J. Pharm. Sci.* **1995,** 84, 966-974.

24. Riecke, E., Spezielle Fälle von Gleichgewichterscheinungen eines aus mehreren Phasen zusammengesetzten Systemes. *Z. Phys. Chem. (Munich)* **1890,** 6, 411-429.

25. ACDLabs *Advanced Chemistry Development (ACD/Labs) Software*, V11.02; ACD/Labs.

26. Ceolin, R.; Allouchi, H.; Rietveld, I. B., On the dimorphism and the pressure-temperature state diagram of gestodene, a steroidal progestogen contraceptive. *Ann Pharm Fr* **2020,** 78, 303-309.

27. Ceolin, R.; Rietveld, I.-B., X-ray crystallography, an essential tool for the determination of thermodynamic relationships between crystalline polymorphs. *Ann. Pharm. Fr.* **2016,** 74, 12-20.

28. Toscani, S.; de Oliveira, P.; Céolin, R., Phenomenology of polymorphism IV. The trimorphism of ferrocene and the overall metastability of its triclinic phase. *J. Solid State Chem.* **2002,** 164, 131-137.

29. Toscani, S.; Céolin, R.; Ter Minassian, L.; Barrio, M.; Veglio, N.; Tamarit, J.-L.; Louër, D.; Rietveld, I. B., Stability hierarchy between piracetam forms I, II, and III from experimental pressure-temperature diagrams and topological inferences. *Int. J. Pharm.* **2016,** 497, 96-105.

30. Nicolai, B.; Barrio, M.; Lloveras, P.; Polian, A.; Itie, J. P.; Tamarit, J. L.; Rietveld, I. B., A thermodynamically consistent phase diagram of a trimorphic pharmaceutical, l-tyrosine ethyl ester, based on limited experimental data. *Phys Chem Chem Phys* **2018,** 20, 24074-24087.

31. Barrio, M.; de Oliveira, P.; Céolin, R.; Lopez, D. O.; Tamarit, J. L., Polymorphism of 2-methyl-2-chloropropane and 2,2-dimethylpropane (neopentane): Thermodynamic evidence for a high-pressure orientationally disordered rhombohedral phase through topological p-T diagrams. *Chem. Mater.* **2002,** 14, 851-857.